Mon. Not. R. Astron. Soc. **389,** 1391–1398 (2008) doi:10.1111/j.1365-2966.2008.13659.x

On the genealogy of the Orphan Stream

Laura V. Sales,[1★] Amina Helmi,[1] Else Starkenburg,[1] Heather L. Morrison,[2] Ethan Engle,[2] Paul Harding,[2] Mario Mateo,[3] Edward W. Olszewski[4] and Thirupathi Sivarani[5]

[1]*Kapteyn Astronomical Institute, University of Groningen, PO Box 800, 9700AV Groningen, the Netherlands*
[2]*Department of Astronomy, Case Western Reserve University, Cleveland, OH 44106-7215, USA*
[3]*Department of Astronomy, University of Michigan, Ann Arbor, MI 48109, USA*
[4]*Steward Observatory, University of Arizona, Tucson, AZ 85721, USA*
[5]*Department of Physics & Astronomy and JINA: Joint Institute for Nuclear Astrophysics, Michigan State University, MI, USA*

Accepted 2008 June 27. Received 2008 June 20; in original form 2008 May 5

ABSTRACT

We use *N*-body simulations to explore the origin and a plausible orbit for the Orphan Stream, one of the faintest substructures discovered so far in the outer halo of our Galaxy. We are able to reproduce its position, velocity and distance measurements by appealing to a *single* wrap of a double-component satellite galaxy. We find that the progenitor of the Orphan Stream could have been an object similar to today's Milky Way dwarfs, such as Carina, Draco, Leo II or Sculptor; and unlikely to be connected to Complex A or Ursa Major II. Our models suggest that such progenitors, if accreted on orbits with apocentres smaller than ∼35 kpc, are likely to give rise to very low surface brightness streams, which may be hiding in the outer halo and remain largely undetected with current techniques. The systematic discovery of these ghostly substructures may well require wide field spectroscopic surveys of the Milky Way's outer stellar halo.

Key words: galaxies: evolution – galaxies: formation – galaxies: haloes – galaxies: kinematics and dynamics.

1 INTRODUCTION

Tidal streams represent direct signatures of the merging history of galaxies. In cold dark matter (CDM) models, structures grow in a bottom-up fashion, by the accretion of smaller subunits. After entering in the gravitational domain of a larger system, tides effectively remove material from the satellites, creating 'tails' of particles, either dark matter, gas or stars that approximately trace the orbits of their progenitors. The existence of tidal streams in the haloes of galaxies would therefore be a natural expectation in the hierarchical paradigm of structure formation.

However, it is still unclear how fundamental or dominant mergers have been in the build-up of our Galaxy. In a recent paper, Bell et al. (2007) found that the amount of substructure in the Milky Way's halo is consistent with the most extreme scenario, in which it was *entirely* formed from the accretion of satellites.

Although a large amount of stellar streams are predicted in these hierarchical models (Johnston, Spergel & Hernquist 1995; Johnston 1998; Helmi & White 1999; Bullock, Kravtsov & Weinberg 2001; Helmi, White & Springel 2003; Bullock & Johnston 2005), detection is generally difficult due to their low surface brightness and low contrast against Galactic field stars. This implies that our own Galaxy and also our closest neighbour, M31, may offer the best chances for identifying streams in stellar surveys. Perhaps the clearest and best-known example is the Sagittarius Stream, discovered about a decade ago. With the advent of large wide-field surveys like 2MASS (Skrutskie et al. 2006) and the Sloan Sky Digital Survey (SDSS, York et al. 2000; Adelman-McCarthy et al. 2007) it was possible to trace this stream out to 360° on the sky (Majewski et al. 2004), allowing the modelling of the orbit and intrinsic properties of its progenitor, the Sagittarius dwarf (Helmi & White 2001; Ibata et al. 2001b; Helmi 2004; Martínez-Delgado et al. 2004; Fellhauer et al. 2006). Also M31 shows a prominent 'Giant Arc', a stellar stream of average surface brightness $\Sigma_V \sim 30$ mag arcsec^{-2}, whose progenitor has not yet been confirmed (Ibata et al. 2001a; Fardal et al. 2006; Font et al. 2006; Guhathakurta et al. 2006; Kalirai et al. 2006; Gilbert et al. 2007). Therefore, these surveys have consolidated the idea that the stellar haloes of M31 and the Galaxy may well be highly lumpy components. This appears to also be the case for galaxies beyond the Local Group, as recent studies have shown (e.g. Martinez-Delgado et al. 2008, and references therein).

Stellar streams are useful tracers of their progenitor's orbit, due to their coherence in phase space. This property allows us in some cases to link a given tidal feature with its parent satellite; for instance, by extrapolation of its great circle on the sky (Lynden-Bell

★E-mail: lsales@astro.rug.nl LVS

© 2008 The Authors. Journal compilation © 2008 RAS

& Lynden-Bell 1995). At the same time, tidal streams also hold essential clues about the object in which they originated, as their luminosity and cross-section are directly related to the mass and velocity dispersion of their progenitors (Johnston 1998). Stream properties also depend on the time of disruption, since the material that is stripped off earlier in time tends to become broader, and hence, to have lower surface brightness as time goes by (Helmi & White 1999). In this context, we naturally expect an observational bias towards detecting remnants of *recent* accretion events involving *massive* progenitors, as the case of the Sagittarius stream in the Milky Way or the Giant Arc in M31. However, an unusually narrow and faint stream discovered in our Galaxy stands out from this general trend. The Orphan Stream (Grillmair 2006; Belokurov et al. 2007a) with only ∼0.70 kpc of full width half-mass (FWHM) projected on the sky, is about approximately five times narrower than the Sagittarius Stream, and has a surface brightness which is about a factor ∼2 lower. Given its atypical properties, the Orphan Stream provides us with the opportunity of studying the fainter end of the family of objects that built up the stellar halo of our own Galaxy.

As highlighted by its name, the Orphan Stream progenitor has not yet been identified, although its properties (mainly cross-section and luminosity) seem to favour a dwarf-like object rather than a globular cluster. Some attempts have been made to link this stream to other known objects of our Galaxy. Belokurov et al. (2007b), based on the paths defined by great circles on the sky (a technique first developed by Lynden-Bell & Lynden-Bell 1995), highlighted a potential connection of the stream with several globular clusters (Palomar 1, Arp2, Terzan 7 and Segue 1), as well as to the recently discovered faint dwarf galaxy, Ursa Major II (UMa II, Zucker et al. 2006b). In a later paper, Fellhauer et al. (2007) used numerical simulations to test the likely association between the Orphan Stream and UMa II. These authors propose a model in which both objects have a common origin, also allowing for a physical association of the stream with a set of high velocity clouds named Complex A. However, this model requires the stream to be the result of the exact overlap on the sky of two independent wraps, which at face value appears somewhat contrived given its noticeable cohesion.

In a novel approach, Jin & Lynden-Bell (2007) exploited the possible relation of Complex A with the stream to estimate its average distance. However, the method under-predicts the distances by a factor of ∼3, also disfavouring the scenario in which the Orphan Stream and Complex A share the same orbit.

This paper presents a new attempt to find a plausible orbit for the Orphan Stream progenitor, that is able to reproduce the current position and velocity measurements appealing to only one wrap; as suggested by the coherence observed in the images of the stream. Our model for the progenitor aims to be consistent with dwarf spheroidal galaxies, like those found orbiting the Milky Way today. The paper is organized as follows. We describe the simulations as well as the progenitor model in Section 2, we present the results and discussion in Sections 3 and 4. Finally, we summarize our main conclusions in Section 5.

2 NUMERICAL MODELLING

We use the *N*-body code GADGET-2 (Springel 2005)[1] to study the evolution of a two-component satellite galaxy orbiting in the (fixed) gravitational potential of the Milky Way. We model the Galactic potential as follows.

(i) A spherical NFW (Navarro, Frenk & White 1996, 1997) dark matter halo:

$$\rho(x = r/r_{\rm vir}) \propto \frac{1}{x(1+cx)^2}$$

with mass $M_{\rm vir} = 1 \times 10^{12}\,{\rm M}_\odot$, concentration $c = 12$ and virial radius $r_{\rm vir} = 258$ kpc (Klypin et al. 2002),

(ii) A Hernquist bulge:

$$\rho(r) = \frac{M_{\rm blg} a_{\rm b}}{2\pi r}\frac{1}{(r+a_{\rm b})^3}$$

with mass $M_{\rm blg} = 3.4 \times 10^{10}\,{\rm M}_\odot$ and scale length $a_{\rm b} = 0.7$ kpc,

(iii) A Miyamoto-Nagai disc:

$$\rho(R,z) = \frac{b^2 M_{\rm dsk}}{2\pi}\frac{aR^2 + (a+3\sqrt{z^2+b^2})(a+\sqrt{z^2+b^2})^2}{[R^2+(a+\sqrt{z^2+b^2})^2]^{5/2}(z^2+b^2)^{3/2}}$$

with parameters $M_{\rm dsk} = 1 \times 10^{11}\,{\rm M}_\odot$, $a = 6.5$ kpc and $b = 0.26$ kpc (Johnston, Sigurdsson & Hernquist 1999).

The composite circular velocity at the solar distance is $V_{\rm c} = 220\,{\rm km\,s^{-1}}$ in agreement with observations. The circular velocity at the virial radius is $V_{\rm c}(r_{\rm vir}) = V_{\rm vir} = 136\,{\rm km\,s^{-1}}$. Note that for simplicity we have assumed a spherical dark matter halo, and that the mass distribution is time independent. This assumption is justified because the gravitational potential inside the orbit of the Orphan Stream (<40 kpc, see next section) is unlikely to have changed significantly in the recent past because of the presence of a relatively old thin disc. On the other hand Peñarrubia et al. (2006) suggest that the properties of tidal streams mainly reflect the *present-day* potential of the primary halo and are not fundamentally affected by its growth in time.

Our model of the satellite has two spherical components: an extended dark matter halo and a more concentrated 'luminous' component (see middle and right-hand panels of Fig. 1). Dark matter particles are distributed following a Hernquist profile of mass $M^{\rm sat}_{\rm drk} = 2.5 \times 10^8\,{\rm M}_\odot$ and characteristic scale $a_{\rm sat} = 0.9$ kpc. The circular velocity of the dark halo peaks at $r_{\rm max} \sim 0.75$ kpc reaching $V_{\rm max} \sim 20\,{\rm km\,s^{-1}}$ (see left-hand panel of Fig. 1), and hence would be consistent with the properties of the Milky Way dwarf spheroidals Peñarrubia et al. (2007, 2008). The second component mimics the stellar content of a dwarf galaxy and is represented by a Plummer profile of mass $M^{\rm sat}_{\rm str} = 7.5 \times 10^5\,{\rm M}_\odot$ and characteristic scale $b_{\rm sat} = 0.1$ kpc. The half light radius of our model satellite is $r_{\rm h} \sim 0.13$ kpc and its central velocity dispersion is $\sigma_0 \sim 7\,{\rm km\,s^{-1}}$.

We used the web-tool BaSTI[2] to generate isochrones and convert the stellar mass ($M_{\rm str} = 7.5 \times 10^5\,{\rm M}_\odot$) to the luminosity of our modelled satellite. Given the typically old stars present in dwarfs galaxies, and assuming a single population of 10 Gyr and [Fe/H]~ -2 dex, the conversion factor we obtain is $\gamma \sim 2.9$. This gives a total luminosity for the progenitor in our simulations of $L \sim 2 \times 10^5\,{\rm L}_\odot$, consistent with the luminosity of dwarf spheroidals in the Local Group. This object is dark matter dominated, with a mass-to-light ratio $\gamma \sim 39$ measured within the half light radius. With these parameters the model is comparable to several classical dwarfs, such as Carina, Leo II or Sculptor.

[1] http://www.mpa-garching.mpg.de/∼volker/gadget/index.html

[2] www.te.astro.it/BASTI/index.php

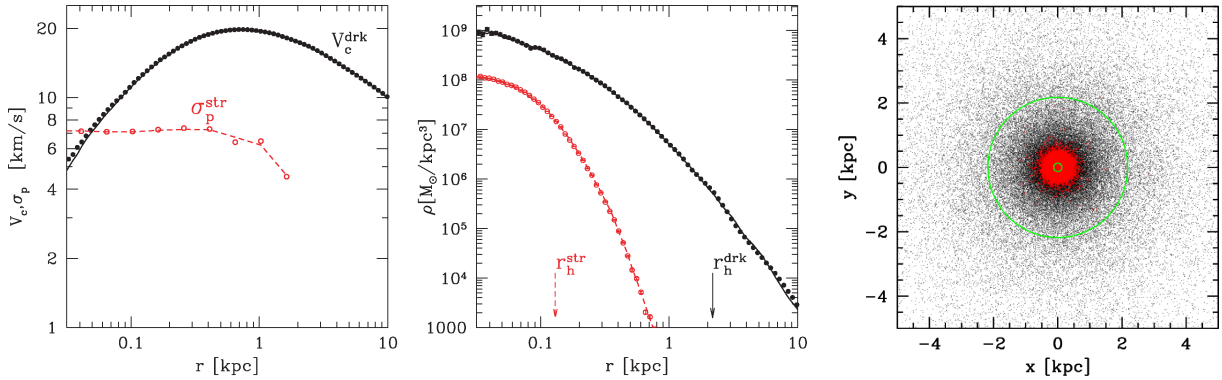

Figure 1. Properties of the satellite model considered in this work. Left-hand panel: dark matter circular velocity (black squared dots, solid line) and the (projected) velocity dispersion of the luminous component (open red circles, dashed line) of the satellite as a function of radius. Lines indicate the profiles as set up in the initial conditions, while points show these quantities after the model is relaxed in isolation during 2 Gyr. Middle panel: dark and luminous matter density profiles for the satellite, arrows show the half-mass radii for each component. Lines and points are colour-coded as in the previous panel. Right-hand panel: projected positions of the dark matter (black) and luminous (red) particles in the relaxed satellite model. The green circles indicates the half-mass radius, highlighting the appreciable segregation of the stars with respect to the dark halo.

The number of particles used in our simulations are 5×10^5 and 2×10^5 for the dark and stellar components, respectively. We use an unequal softening scheme, with a Plummer-equivalent softening length $\epsilon_{DM} = 0.04$ kpc and $\epsilon_{str} = 0.004$ kpc for the dark matter and luminous component, respectively. We set up the initial conditions following the procedure outlined by Hernquist (1993), aimed to generate multicomponent systems in dynamical equilibrium. The satellite is first evolved in isolation during 2 Gyr (∼200 crossing times for a particle at the half-light radius, while for one at the edge, that is, at 5 kpc from the centre, this corresponds to approximately five crossing times), where it is allowed to relax. Then, the satellite was put on its current orbit in the fixed Milky Way potential.

As stated above, our model for the Orphan Stream progenitor could well represent one of the 'classical' Milky Way dwarf galaxies, where 'classical' is used to distinguish the first eleven discovered satellites around our Galaxy (Mateo 1998; van den Bergh 1999), from the more recently identified SDSS dwarfs (Zucker et al. 2004; Willman et al. 2005; Martin et al. 2006; Belokurov et al. 2006; Zucker et al. 2006a,b; Belokurov et al. 2007b; Irwin et al. 2007; Majewski et al. 2007; Simon & Geha 2007). These new dwarfs are typically ∼100 times less luminous, but with comparable half light radii (∼80–500 pc) and velocity dispersion (∼4–8 km s^{-1}). Therefore, their surface brightness is appreciably lower (∼28–30 mag arcsec^{-2}) and their mass-to-light ratio is ∼10–50 times higher. One of the strongest constraints on the Orphan Stream progenitor comes from its total luminosity. Belokurov et al. (2007b) estimate that the total *r*-band absolute magnitude for the (visible) portion of the stream is $M_r \sim -6.7$. Since leading and trailing arms should have comparable mass, a lower limit to the total luminosity is roughly $L \sim 10^5$ L$_\odot$, ruling out practically all new SDSS dwarfs as suitable candidates.[3]

3 RESULTS

It is not possible to fully constrain the orbit of the Orphan Stream with only the available radial velocity and distance information. Proper motion measurements would be needed to that end. However, given that the stream extends ∼55° on the sky, it is possible to find a suitable orbit by requiring that it should pass through both ends of the observed stream, with the measured (although preliminary) radial velocities and distances. This can be done by requiring that the total angular momentum of both ends of the stream be the same (for example, the orientation of the orbital plane is constrained by the cross-product of the position vectors of the stream end-points). With this condition, we randomly generate possible orbits that match (within the errors) all observables.

The satellite is placed at one apocentre of such an orbit, from where we follow its subsequent evolution within the Milky Way's gravitational field. The orbit is confined to the inner 40 kpc of the Galaxy halo (apocentre: $r_{apo} = 38$ kpc, pericentre: $r_{per} = 7$ kpc); where the gradient of the potential is large, producing strong tides that fully disrupt the progenitor in less than ∼3.5 Gyr. The snapshot view with the final distribution of satellite particles after 5.3 Gyr is shown in Fig. 2. The box is 100 kpc on a side and the projection is along the *x*-coordinate. The green rectangle shows the portion of the stellar trail that would represent the Orphan Stream in our model. The distribution of dark matter (black dots) is broad and shows no spatial coherence. Due to its more extended distribution, dark matter particles are stripped off first, and hence this debris is dynamically older, and consequently more diffuse. However, we can still identify by eye a few shells or 'caustics' that outline the turn-around points along the orbit (Hernquist & Quinn 1987, 1988; Helmi & White 1999).

The luminous component of our satellite is a factor ∼17 more concentrated (the ratio of their half mass radii is: $r_h^{drk}/r_h^{str} = 16.7$), which makes its core more resilient to tidal disruption than the extended dark matter. Nevertheless, after the second pericentre passage, the first stellar trails are produced (at which point the satellite has lost more that 95 per cent of its initial dark matter content). The stellar streams hence grow at the expense of the satellite's pruning, a process that, if strong and enduring enough, drives to the irreversible disruption of the object.

Note that we have followed the evolution of the model satellite for 5.3 Gyr. This time-scale is partly driven by the initial properties of the satellite and by our desire to reproduce the current properties of the stream. As discussed in detail in Section 3.3, this choice is not unique as strong dependencies between the initial conditions

[3] Only the Canes Venatici I dwarf, whose luminosity $L \sim 1.2 \times 10^5$ L$_\odot$ is above this lower limit. However, this galaxy is too extended ($r_h = 0.56$ kpc) to give rise to a stream as narrow as observed.

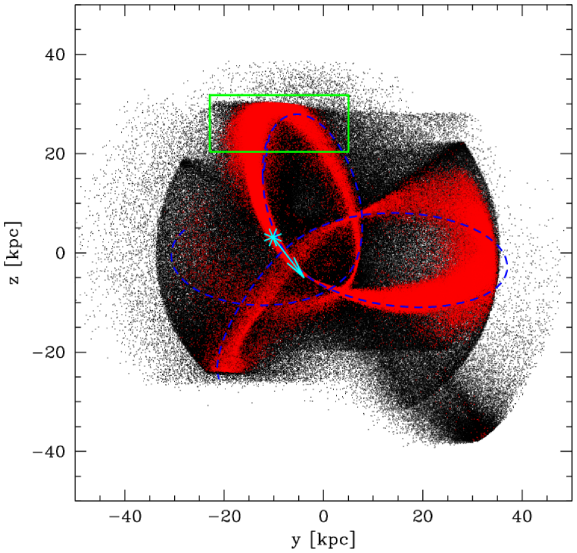

Figure 2. Distribution of dark matter (black) and star particles (red) at 5.3 Gyr after infall. The section matching the Orphan Stream measurements is enclosed by the green rectangle. It sits on the *trailing* arm, traced here (together with the leading arm) by the dashed blue line. The cyan asterisk corresponds to the position of the most bound star particle, with the sense of motion in the orbit shown by the arrow. Dark matter particles are removed from the progenitor at earlier times, causing the stream to be dynamically old and with poor coherence in space, although characteristic 'shells or 'caustics' can still be distinguished in the distribution. On the other hand, star particles are more clumped, approximately tracing the last loop (*trailing* arm) and next loop (*leading* arm) of the orbit.

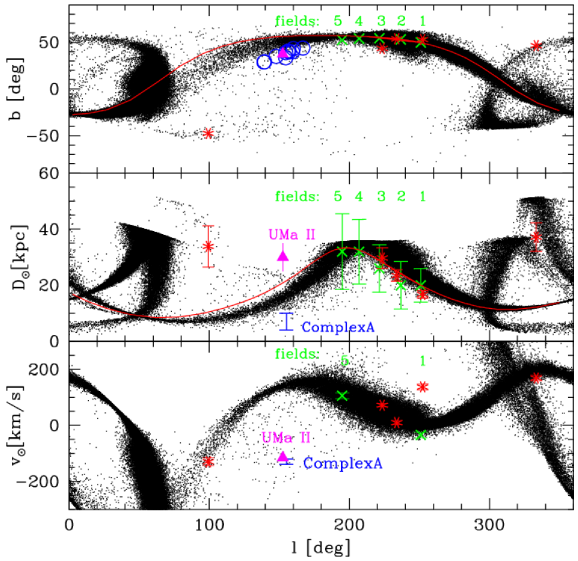

Figure 3. All sky view of the final distribution of stellar particles in our model. We show in the upper panel the projected positions in galactic coordinates (l, b), middle and bottom panels correspond to the heliocentric distances ($D_\odot$) and velocities ($V_\odot$), respectively. The thin red line shows (a portion of) the trajectory of a point-mass on the same orbit as the Orphan Stream progenitor, integrated in the analytic potential of the Milky Way. Green crosses indicate the measurements for the Orphan Stream, fields 1–5 taken from Belokurov et al. (2007b). For comparison with previous works, we also include current estimations for the positions, distances and velocities for Complex A (blue empty circles) and Ursa Major II (Martin et al. 2007; Simon & Geha 2007, magenta filled triangle). Red asterisks show the properties of 5 red giant stars from the Spaghetti survey, probably related to the stream (see Section 4 for further details).

of the model satellite and the integration time exist. None the less, the above choice of an integration time-scale shorter than a Hubble time for a relatively tight orbit may be also justified in light of recent cosmological simulations. These have shown that satellites are often accreted in groups (Li & Helmi 2008), and that through multiple-body interactions acting during the tidal dissociation of such groups their orbits can be changed significantly (Sales et al. 2007; Ludlow et al. 2008). Such events are relatively common, and might explain how our model satellite was put on its current orbit only 5.3 Gyr ago.

3.1 The orbit and the stream global properties

Fig. 3 shows the position on the sky in galactic coordinates, the heliocentric distances and velocities of the star particles in our model, in comparison with the measurements of the Orphan Stream reported by Belokurov et al. (2007b).

In this snapshot, the former centre of mass of the satellite is located at $l = 306.^\circ1$, $b = 13.^\circ9$, at a heliocentric distance of 13 kpc and moving with a velocity of $v_\odot = 97.6\,\mathrm{km\,s^{-1}}$.

The most recent wrap of the orbit is enclosed between galactic latitudes $b = [-30^\circ, +60^\circ]$, and is pretty well traced by the majority of the star particles (see upper panel in Fig. 3). However, we can also see evidence of previous loops, visible as a bulk of particles with $l < 90^\circ$ and also at $l > 280^\circ$. The section of the stream that matches the Orphan Stream observations forms an arc of $\sim 55^\circ$ in the *trailing* arm (the sense of motion in the orbit is pro-grade, that is, towards larger galactic longitudes), where the maximum surface brightness is reached. The leading arm is responsible for the overdensity of particles with $l < 90^\circ$ and also $l \sim 300^\circ$. The different branches are better distinguished in the middle panel of Fig. 3, where the leading arm has a maximum distance of $\sim$40 kpc and the particles in the tip of the trailing arm are located at $l > 320^\circ$ with distances up to $D_\odot \sim 50$ kpc.

Fig. 3 shows that positions, distances and velocities determined for fields 1–5 (Belokurov et al. 2007b) of the Orphan Stream are well reproduced by our model. Our distances might be slightly larger than measured by Belokurov et al. (2007b) in fields 2 and 3, but still in good agreement, especially given the size of the error bars. The velocities are also nicely consistent with the observed values, considering that the latter were determined with barely more than a couple of dozen stars per bin. Although some attempts to improve the observational estimations of the velocities in the Orphan Stream fields have already been made, unfortunately they have not yet succeeded (Belokurov, private communication). Nevertheless, it is clear that a more definitive test to the orbit (and the progenitor) presented in this work will come from better measurements of velocities and smaller distance brackets for each of the fields.

A possible association between the Orphan Stream and Complex A was suggested by Belokurov et al. (2007a), Fellhauer et al. (2007) and Jin & Lynden-Bell (2007). Complex A is a set of high velocity clouds whose position in the sky lies along the best-fitting great circle traced by the Orphan Stream (see fig. 7 in Belokurov et al. 2007a). However, the model presented here shows no connection (in the current as well as in previous loops) between these two objects (see Fig. 3). Our results also do not support an association between the stream and UMa II, as suggested by Fellhauer et al. (2007).

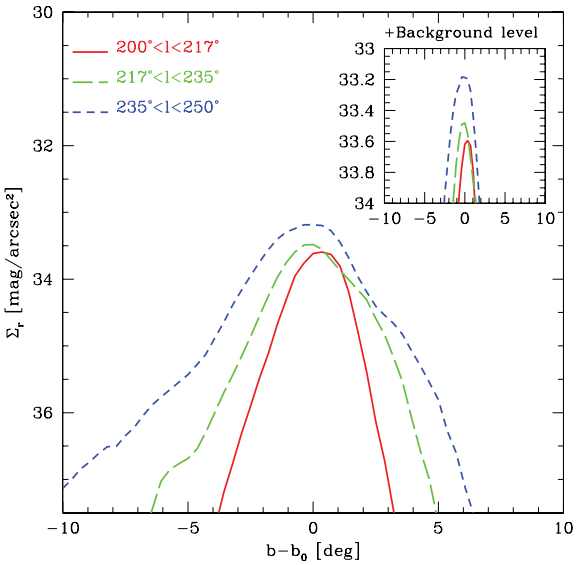

Figure 4. Transverse surface brightness profile of the simulated stream, in the region that matches the location of the Orphan Stream. For each longitude range we re-centred the distribution according to its baricentre latitude, b_0. The main box shows the total distribution of light, while the small indicates the likely 'detection', i.e. the excess of flux over a background surface brightness $\Sigma_r^F = 34\,\mathrm{mag\,arcsec^{-2}}$. As discussed in the text, accounting for the foreground and background contribution helps to reproduce the narrow cross-section of the Orphan Stream shown in SDSS data.

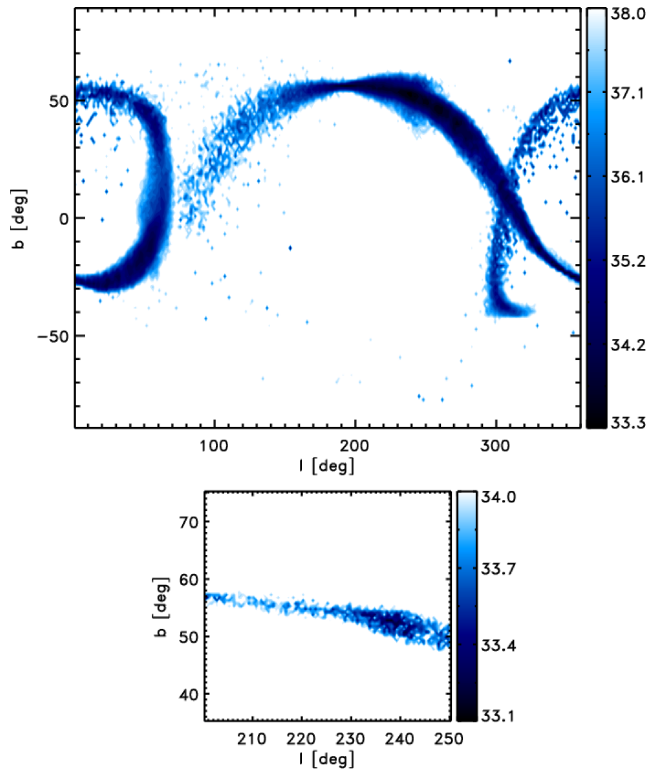

Figure 5. Main box: All-sky surface brightness map of the simulated satellite and its debris, assuming a mass-to-light ratio for star particles of $\gamma = 2.9$ (see text for details). Small box: zoom-in into the Orphan Stream region. Notice the change of scale in the density map. In this box we have considered $\Sigma_r^F = 34\,\mathrm{mag\,arcsec^{-2}}$ as the lower limit in the surface brightness, in order to account for the foreground and background stars on the Milky Way in this region of the sky. The average FWHM of the 'observable' portion of the simulated stream is then $\sim 2^\circ$ in nice agreement with the observations. The trend of increasing number of stars towards larger latitudes is also reproduced in our model.

3.2 Stream intrinsic properties

In the following paragraphs we address how well the intrinsic properties of the Orphan Stream (magnitude, extension, width, etc.) are reproduced in our model:

(i) *Stream width*. One of the peculiarities of the Orphan Stream is its small cross-section ($\sim 2^\circ$), that distinguishes it among its siblings, for example, the Sagittarius Stream or Monoceros Ring. The total width of the model stream in the region $l = [200^\circ, 250^\circ]$ is 15°, significantly wider than what has been reported. However, much of this stream is at such low surface brightness levels that it would remain undetected given the expected background, as shown for example in Fig. 5. To account for the contribution from background and foreground stars we use the Besancon Model[4] 4 (Robin et al. 2003). From this we estimate the number of stars in our Galaxy that are expected within a 15 square degree region of the sky centred at the Orphan Stream's position. We apply the apparent magnitude limit and colour cuts adopted by Belokurov et al. (2007b) (stars with $21 < r < 22$ and $(g - r) < 0.4$); obtaining an r-band surface brightness for the field: $\Sigma_r^F \sim 33.8\,\mathrm{mag\,arcsec^{-2}}$. Therefore, the stream stars would be confused with the background at $\Sigma_r \sim 34\,\mathrm{mag\,arcsec^{-2}}$. When we apply this threshold to our simulation, we find that the 'observable' portion of the stream nicely reproduces the $\sim 2^\circ$ cross-section. This is illustrated in detail in Fig. 4, where we show the average cross-section profiles of the simulated stream and the effect of adding the foreground and background contributions. The final structure of the stream is shown in the bottom panel of Fig. 5.

(ii) *Stream length*. The current detection of the Orphan Stream covers an arc of $\sim 55^\circ$ on the sky. This strongly constrains the time required for the debris to spread in the simulation to a matching extent. For our model we need about ~ 5 Gyr. Shorter time-spans of the modelled satellite in the fixed potential ($t < 4.5$ Gyr) generate streams that are not long enough, while a longer time integration ($t > 6.3$ Gyr) creates tidal streams that are too wide and diffuse compared to the Orphan Stream.

(iii) *Stream luminosity*. The total amount of mass in the simulated stream depends on the limit in the surface brightness we adopt. Applying the threshold given in the observations by the field brightness, Σ_r^F, we obtain $m \sim 1.1 \times 10^5\,\mathrm{M_\odot}$. This translates to a luminosity: $L \sim 2.3 \times 10^4\,\mathrm{L_\odot}$, or an absolute magnitude $M_r \sim -6.4$. These numbers are in very good agreement with Belokurov et al.'s measurements, who estimate $M_r \sim -6.7$. Nevertheless, we notice that the real mass in the stream is twice this number, once the limiting surface brightness considered drops to $\Sigma_r = 38\,\mathrm{mag\,arcsec^{-2}}$ instead of the $\Sigma_r^F = 34\,\mathrm{mag\,arcsec^{-2}}$ imposed by background and foreground stars.

(iv) *Stream gradient*. Our model also reproduces the non-uniformity in the surface brightness of the Orphan Stream. As pointed out by Belokurov et al., the density of stars noticeably increases towards lower latitudes. Bottom panel of Fig. 5 shows that there are approximately twice as many stars in $l > 230^\circ$ (fields 1–2) than for the upper tip $l < 220^\circ$ (fields 4–5). This effect is generated by: (i) fields 1–2 are closer to the former progenitor than the upper

[4] http://bison.obs-besancon.fr/modele/

tip of the stream and (ii) fields 4–5 are 50 per cent farther away from the Sun than the lower section of the stream, compromising even more its detection.

(v) *Final fate of the progenitor.* The large degree of disruption in our model satellite needed to generate an arc on the sky as large as $\sim 55^\circ$ prevents the progenitor to survive as a self-bound entity for more than $t \sim 3$ Gyr. A robust conclusion that we can draw after having explored several models for the satellite, starting from conditions that resemble today's Milky Way dwarfs, is that any remnant at the present time should be very close to (if not already) fully disrupted.

3.3 Model degeneracies

The orbit presented here is likely to be one of many possible ones. This is because of the freedom introduced by the lack of proper motions measurements and the large uncertainties in the radial velocities and distances, as well as by the unknown exact form of the gravitational potential of the Galaxy.

Furthermore, as a final comment in this section, we point out that the uncertainties on the measurements and the lack of an entire sky survey with the resolution of the SDSS, makes the problem of determining the properties of the Orphan Stream progenitor quite degenerate (see Fellhauer et al. 2007 for a similar conclusion). The approach in this paper has been to choose a object that resembles one of today's Milky Way dwarfs. Nevertheless, the solution is not unique.

There are two factors that largely determine the success of a model on the orbit presented here: the central density of the satellite (or the average density within the half-light radius) and the scale of the stellar distribution (see for instance fig. 2 of Peñarrubia et al. 2008). Note that these two factors also determine the stellar velocity dispersion, a quantity that has direct impact on the stream's width.

The satellite's central density determines the likelihood of survival and the degree of disruption of the object on the current orbit. Hence, this will determine how long the streams are and for how long the object has been orbiting the Galaxy. For example, the observations constrain the length of the stream to an arc of 55°. Assuming that the Orphan Stream is actually the brightest section of the total (full-sky) stream, and given that no progenitor has been found close to the region where the stream reaches its peak surface brightness, this implies that the object must be close to (if not) fully disrupted. Therefore the initial average density of the object must be comparable to the density of the host at the pericentre distance ($\sim 3 \times 10^7\,\mathrm{M_\odot\,kpc^{-3}}$). An object with a significantly higher central density will not suffer enough tidal stripping nor shocks to be significantly perturbed and disrupted. An object with a much lower density will be fully disrupted giving rise to streams that are too faint to be observable. This is why a model like ours needs 5.3 Gyr to give rise to an object that is fully disrupted and to streams of the required length. A model with a slightly higher dark-matter density, but the same stellar distribution, would survive longer, and hence the integration time required to reach the present state would also need to be larger. A model with a smaller amount of dark matter near the centre (e.g. reduced by 50 per cent) is also possible, since it does not lead to significant changes in the observables, as long as the satellite evolves for a shorter time in the Milky Way potential (4.7 Gyr instead of 5.3 Gyr).

The second factor that is crucial in our model is the extent of the luminous component, since this determines almost completely the narrowness of the observed streams. In principle, an interplay between a shorter time integration and a more extended progenitor could also provide a suitable model for the stream. However, we were unable to obtain a good match between simulations and observations by using a satellite model as extended as the one proposed by Fellhauer et al. (2007). These authors used a two-component model with similar mass for the luminous particles, but its half light radius is $r_\mathrm{h} \sim 480$ pc, approximately 3.5 times larger than our fiducial progenitor. Such an extended object in our preferred orbit produces a stream that is too wide and with too low surface brightness in comparison to the Orphan Stream. On the other hand, the mass in the luminous component could also be increased maintaining the mass–size relationship observed for the local dwarf spheroidals. However, these more extended progenitors give rise to tails that are too wide and (now) too bright to fit the Orphan Stream observations.

As stated above, these degeneracies are important since the integration time-scale can then be made as long as desired by increasing the average density of the progenitor. For example, one may desire a model which has been on the present orbit around the Galaxy for the past 10 Gyr. By performing numerical experiments we have found that a satellite with a mean density within the half light radius r_h which is 10 times larger than our fiducial model (i.e. $\sim 2.9 \times 10^9\,\mathrm{M_\odot\,kpc^{-3}}$) will achieve after 10 Gyr the level of disruption needed to reproduce the observations. Such a model can be obtained by increasing the dark matter halo mass by a factor 10 while keeping its scale-length a_sat fixed. However, this will lead to a significantly larger stellar velocity dispersion in comparison to the previous model (with $\sim 7\,\mathrm{km\,s^{-1}}$), and hence will fail in reproducing the width of the Stream. Therefore also the extent of the luminous component must be modified to become more concentrated than our fiducial model. The magnitude of this modification can be derived from the following argument based on the initial stellar velocity dispersion of the system σ_str. Since most of the mass is in dark matter, we can neglect the contribution of the stars to the velocity dispersion, and therefore assuming, as before, a Hernquist halo and a Plummer profile for the stars we find:

$$\sigma_\mathrm{str}(r) = GM_\mathrm{drk}\left(r^2 + b_\mathrm{sat}^2\right)^{5/2} \int_r^\infty \frac{1}{\left(x^2 + b_\mathrm{sat}^2\right)^{5/2}} \frac{\mathrm{d}x}{(x + a_\mathrm{sat})^2},$$

where a_sat and b_sat are the characteristic radii of the Hernquist and the Plummer profiles, respectively (Hernquist 1993). The dark halo mass, M_drk is fixed by our requirement of a given central density. If we now vary b_sat we can get a range of velocity dispersions that goes from 4 $\mathrm{km\,s^{-1}}$ if $b_\mathrm{sat} = 20$ pc up to $\sim 24\,\mathrm{km\,s^{-1}}$ for $b_\mathrm{sat} = 0.1$ kpc as before. If we use our fiducial model as a guide, the new model integrated for 10 Gyr will be successful if $\sigma_\mathrm{str} \sim 7\,\mathrm{km\,s^{-1}}$ after ~ 5 Gyr of evolution. Since disruption causes the velocity dispersion to drop, models with initial σ_str in the range 9–12 $\mathrm{km\,s^{-1}}$ will generate the kind of progenitor we are looking for. According to the equation above, that corresponds to a half light radius $r_\mathrm{h} \sim$ 50–65 pc.

This new progenitor should also fulfil the constraints in luminosity given by the brightness of the visible portion of the Orphan Stream (see Section 2), which implies $L \geq 10^5\,\mathrm{L_\odot}$. Therefore, we find that by fixing the central density, and changing the parameters of the luminous component accordingly, we can generate a family of progenitors that are roughly consistent with today dwarfs satellites. On this basis, we conclude that models evolving for 5–10 Gyr and with the properties specified above could represent feasible candidates to the progenitor of the Orphan Stream.

For completeness, we have also explored single-component (no dark matter) models (reminiscent of a globular cluster or a dwarf galaxy that has already lost its subhalo) as tentative progenitors for the stream. We find that such objects should be more concentrated

(typically half light radius ∼40 pc) and need to be integrated for a longer time (∼6.5 Gyr) than our fiducial model, in order to reproduce the length and width of the Orphan Stream. As discussed above, a higher density progenitor could be integrated for a longer time-scale leading to a similar configuration. It is interesting to note that an object like a globular cluster has too high a central density ($\sim 10^{12}\,\mathrm{M}_{\odot}\,\mathrm{kpc}^{-3}$) to be fully disrupted within a Hubble time on this orbit. The amount of mass in the currently detected stream is fixed from observations, hence, the total luminosity of these models should also be $L > 2 \times 10^5\,\mathrm{L}_{\odot}$, as in the double-component case. Progenitors with such properties could be considered unlikely given the properties of the satellites in the Local Group: they are too bright and extended to be a globular cluster and too compact to represent a Milky Way dwarf galaxy (see for instance fig. 10 of Peñarrubia et al. 2008). Therefore, although we cannot rule out a single-component progenitor with such characteristics (since today's satellites might not be representatives of earlier accreted ones); the lack of observations of similar objects turns the dark-matter dominated model presented before a more suitable candidate for our analysis.

4 PRELIMINARY PREDICTIONS AND FUTURE DETECTION PROSPECTS

The upper panel of Fig. 5 shows a dense enough section of the stream, likely identifiable with the current sensitivity of the SDSS; although unfortunately, sitting outside its coverage area. This new stretch contains about approximately two times less stars and traces an arc of ∼35° following the current Orphan Stream detection. It extends from $l = 250°$ to ∼290° in the north galactic hemisphere. The leading arm could in principle be also identified in a survey covering the southern galactic hemisphere. However, its position towards the galactic centre ($l = [-60°, 70°]$) and its lower latitude ($b = [-30°, 10°]$) might compromise the chances of positive imaging detection. In addition to this, its mean surface brightness is on average lower than that of the trailing arm, where the Orphan Stream sits. This difference can be attributed to the fact that the portion of the trailing arm identified as the Orphan Stream lies close to apocentre of the orbit, where the spacial coherence of particles is locally enhanced (e.g. formation of shells or caustics seen in Fig. 2) reaching the maximum surface brightness across the full sky.

An interesting alternative to these photometric approaches, is offered by studies involving also stellar kinematics. Stars remain coherent in velocity space as a consequence of the conservation of phase-space density (Helmi & White 1999), enhancing the correlations of their dynamical parameters.

One relevant study of stellar kinematics of (outer) halo stars is provided by the Spaghetti Survey. This pencil-beam survey of high-latitude fields, first described in Morrison et al. (2000), uses solely red giants as distant halo tracers. The final data set consists of 102 spectroscopically confirmed giants (Starkenburg et al.in preparation). We find five giants within this data set that could be related to the stream in our model (shown by the red asterisks in Fig. 3). Three of them are located right on top of the Orphan Stream fields as detected in Sloan. For two of these, the projected positions, distances and also heliocentric velocities in good agreement with the simulations, indicating a large probability of a real physical link to the stream. The case for the third giant is less clear, since its position agrees with the model, but its velocity is too large (given the radial velocities measured by Belokurov et al. (2007a) are still preliminary, it is possible that this giant is physically related to the Orphan Stream, but not in our model). The remaining two giant stars could belong to different wraps, although they sit on relatively low-density portion of the stream. Table 1 quotes the positions, velocities and metallicities of the selected giants measured by the Spaghetti survey, together with our assessment of the likelihood of membership to the Orphan Stream progenitor according to our simulations.

While red giant surveys like the Spaghetti Survey may be suitable to find stream members and constrain the stream's properties such as radial velocity, the number of detectable candidates is strongly limited by the surface brightness of the stream. The approximate surface brightness of ∼32.4 mag arcsec^{-2} (Belokurov et al. 2007b) transforms to barely 1.3 giants per square degree (Morrison 1993). With more fields on the stream and a more careful analysis of the existing SDSS spectra for giant candidates in fields on the stream, it should be possible to constrain the radial velocities better. However, even fainter substructures might need other tracers such as main sequence stars to determine their properties.

Note also that some sections of the stream in our simulations fall relatively close to the sun (heliocentric distances of the order of 5 kpc) and could, in principle, be accessible to RAVE (Steinmetz et al. 2006). Measurements of the proper motions of the stars associated to the stream could also be used to falsify our model. The orbit presented here as $(\mu_\alpha, \mu_\delta) \sim (-0.10, -2.42)\,\mathrm{mas\,yr}^{-1}$ at $\alpha = 162°$ and $\delta = 0°$, that is, on Field 1. These are within reach of future astrometric missions like GAIA.

5 SUMMARY AND CONCLUSIONS

We have presented *N*-body simulations that reproduce the properties of the recently discovered Orphan Stream. We have studied an orbit able to match, the positions, velocities and distances of the stream. The orbit is in good agreement with the continuous nature of the stream, which may well be a single wrap of the trailing arm of a fully disrupted satellite. The main features of the stream, such as length, cross-section, luminosity and surface brightness are also recreated successfully in the model. However, the orbit does not

Table 1. Galactic coordinates, distances, velocities and metallicities of the Spaghetti Survey giants shown in Fig. 3.

Location	l (°)	b (°)	$\mathrm{D}_\odot$ (kpc)	$\Delta_{\mathrm{D}_\odot}$ (kpc)	$\mathrm{V}_\odot$ (km s^{-1})	$\Delta_{\mathrm{V}_\odot}$ (km s^{-1})	Z (dex)	Δ_Z (dex)	Membership
Field 3	223.45	43.44	29.71	3.71	71.8	5.5	−1.38	0.27	Likely
Field 2	233.83	53.71	23.46	2.03	9.6	7.5	−1.24	0.26	Likely
Field 1	252.28	52.98	16.72	1.39	137.1	10.1	−1.24	0.26	Unlikely
Older wrap	99.38	−47.59	33.88	7.37	−129.9	14	−1.60	0.59	Possible
Older wrap	333.34	46.50	37.16	5.10	168.7	10.1	−1.72	0.27	Possible

Note. Errors in the quantities are also quoted. The last column denotes how consistent the membership to the Orphan Stream progenitor is according to our model.

provide an obvious association of the stream with Complex A or UMa II, as had been suggested previously by Jin & Lynden-Bell (2007) or Fellhauer et al. (2007).

The satellite in our model consists of two components: an extended dark matter halo within which the stars are deeply embedded. We find that the Orphan Stream progenitor could have been an object that resembles one of today's Milky Way dwarfs, such as Carina, Leo II, Draco or Sculptor, and hence, likely to be dark matter dominated. The model predicts the total disruption of this object in order to generate the $\sim 55^\circ$ stellar stream needed to match the observations. This indirectly implies that objects with the properties of the above-mentioned dwarfs can only survive as self-gravitating systems today, because they populate the outer regions of the Galaxy potential, where the gravitational forces are smaller, and the dynamical times of the orbits are longer.

The Orphan Stream distinguishes itself from the previously known tidal features (e.g. Sagittarius Stream or Monoceros Ring in our Galaxy, or the Giant Arc in Andromeda) by its small cross-section. With an average width of $\sim 2^\circ$ it is about approximately five times narrower than the Sagittarius Stream. However, as argued above, this does not imply that its progenitor is an exceptional object. Such streams may therefore be far more common than suspected thus far. The visible strip of the stream may also be just the 'tip of the iceberg', where the amount of mass under our detection limit could be at least twice the current estimation.

We conclude that additional discoveries of tidal features such as the Orphan Stream are fundamental to our understanding of the outer halo of galaxies, as well as to tests of current cosmological models. The detectability of such coherent but very faint structures is compromised not only by the initial luminosity of their progenitors, but also by the dynamical ages of these structures, since they become fainter as they age and diffuse away. The design of techniques to recover these ghostly features needs to be carefully thought out, in order to enable the detection of streams from objects originally populating the faint end of the luminosity function. Future panoramic surveys of the Milky Way stars, as well as the determination of their kinematics, ages and metallicities will play a fundamental role in the Galactic astronomy of the next decades, helping to unveil the secrets recorded in the stellar halo of our own Galaxy.

ACKNOWLEDGMENTS

LVS would like to thank Donald Lynden-Bell, Vasily Belokurov, Nicolas Martin, Mario G. Abadi and Julio F. Navarro for very helpful discussions, as well as to Vibor Jelić for his help with IDL macros. LVS and AH gratefully acknowledge NWO and NOVA for financial support. HLM was supported by NSF grants AST-0098435 and AST-0607518. EO is partially supported by NSF grants AST-0205790 and AST-0507511. TS acknowledges funding from Physics Frontiers Centre/Joint Institute for Nuclear Astrophysics (JINA), awarded by the U.S. National Science Foundation. We also thank the anonymous referee for useful suggestions and comments that helped to improve the previous version of the paper.

REFERENCES

Adelman-McCarthy J. K. et al., 2007, ApJS, 172, 634
Bell E. F. et al., 2007, 706, preprint
Belokurov V. et al., 2006, ApJ, 647, L111
Belokurov V. et al., 2007a, ApJ, 658, 337
Belokurov V. et al., 2007b, ApJ, 654, 897
Bullock J. S., Johnston K. V., 2005, ApJ, 635, 931
Bullock J. S., Kravtsov A. V., Weinberg D. H., 2001, ApJ, 548, 33
Fardal M. A., Babul A., Geehan J. J., Guhathakurta P., 2006, MNRAS, 366, 1012
Fellhauer M. et al., 2006, ApJ, 651, 167
Fellhauer M. et al., 2007, MNRAS, 375, 1171
Font A. S., Johnston K. V., Guhathakurta P., Majewski S. R., Rich R. M., 2006, AJ, 131, 1436
Gilbert K. M. et al., 2007, ApJ, 668, 245
Grillmair C. J., 2006, ApJ, 645, L37
Guhathakurta P. et al., 2006, AJ, 131, 2497
Helmi A., 2004, ApJ, 610, L97
Helmi A., White S. D. M., 1999, MNRAS, 307, 495
Helmi A., White S. D. M., 2001, MNRAS, 323, 529
Helmi A., White S. D. M., Springel V., 2003, MNRAS, 339, 834
Hernquist L., 1993, ApJS, 86, 389
Hernquist L., Quinn P. J., 1987, ApJ, 312, 1
Hernquist L., Quinn P. J., 1988, ApJ, 331, 682
Ibata R., Irwin M., Lewis G., Ferguson A. M. N., Tanvir N., 2001a, Nat, 412, 49
Ibata R., Irwin M., Lewis G. F., Stolte A., 2001b, ApJ, 547, L133
Irwin M. J. et al., 2007, ApJ, 656, L13
Jin S., Lynden-Bell D., 2007, MNRAS, 378, L64
Johnston K. V., 1998, ApJ, 495, 297
Johnston K. V., Spergel D. N., Hernquist L., 1995, ApJ, 451, 598
Johnston K. V., Sigurdsson S., Hernquist L., 1999, MNRAS, 302, 771
Kalirai J. S., Guhathakurta P., Gilbert K. M., Reitzel D. B., Majewski S. R., Rich R. M., Cooper M. C., 2006, ApJ, 641, 268
Klypin A., Zhao H., Somerville R. S., 2002, ApJ, 573, 597
Li Y.-S., Helmi A., 2008, MNRAS, 385, 1365
Ludlow A. D., Navarro J. F., Springel V., Jenkins A., Frenk C. S., Helmi A., 2008, preprint (arXiv:0801.1127)
Lynden-Bell D., Lynden-Bell R. M., 1995, MNRAS, 275, 429
Majewski S. R. et al., 2004, AJ, 128, 245
Majewski S. R. et al., 2007, ApJ, 670, L9
Martin N. F., Ibata R. A., Irwin M. J., Chapman S., Lewis G. F., Ferguson A. M. N., Tanvir N., McConnachie A. W., 2006, MNRAS, 371, 1983
Martin N. F., Ibata R. A., Chapman S. C., Irwin M., Lewis G. F., 2007, MNRAS, 380, 281
Martínez-Delgado D., Gómez-Flechoso M. Á., Aparicio A., Carrera R., 2004, ApJ, 601, 242
Martinez-Delgado D., Pohlen M., Gabany R. J., Majewski S. R., Penarrubia J., Palma C., 2008, 801, preprint (arXiv:0801.4657)
Mateo M. L., 1998, ARA&A, 36, 435
Morrison H. L., 1993, AJ, 106, 578
Morrison H., Mateo M., Olszewski E., Harding P., Dohm-Palmer R., Freeman K., Norris J., Morita M., 2000, AJ, 119, 2254
Navarro J. F., Frenk C. S., White S. D. M., 1996, ApJ, 462, 563
Navarro J. F., Frenk C. S., White S. D. M., 1997, ApJ, 490, 493
Peñarrubia J., Benson A. J., Martínez-Delgado D., Rix H. W., 2006, ApJ, 645, 240
Peñarrubia J., McConnachie A. W., Navarro J. F., 2007, ApJ, 672, 904
Penarrubia J., Navarro J. F., McConnachie A. W., 2008, ApJ, 673, 226
Robin A. C., Reylé C., Derrière S., Picaud S., 2003, A&A, 409, 523
Sales L. V., Navarro J. F., Abadi M. G., Steinmetz M., 2007, MNRAS, 379, 1475
Simon J. D., Geha M., 2007, ApJ, 670, 313
Skrutskie M. F. et al., 2006, AJ, 131, 1163
Springel V., 2005, MNRAS, 364, 1105
Steinmetz M. et al., 2006, AJ, 132, 1645
van den Bergh S., 1999, A&Ar, 9, 273
Willman B. et al., 2005, ApJ, 626, L85
York D. G. et al., 2000, AJ, 120, 1579
Zucker D. B. et al., 2004, ApJ, 612, L121
Zucker D. B. et al., 2006a, ApJ, 650, L41
Zucker D. B. et al., 2006b, ApJ, 643, L103

This paper has been typeset from a TEX/LATEX file prepared by the author.